IAF-01-J.3.03

PRELIMINARY RESULTS OF THE SOUNDING ROCKET EXPERIMENT ON OSCILLATORY MARANGONI FLOWS IN LIQUID BRIDGE

R. SAVINO, R. MONTI, M. LAPPA

Università degli studi di Napoli "Federico II"
Dipartimento di Scienza e Ingegneria dello Spazio "L. G. Napolitano"
P. le V.Tecchio 80, 80125 Napoli (Italy)

D. CASTAGNOLO, R. FORTEZZA

MARS Center
Via Emanuele Gianturco 31, 80142 Napoli (Italy)

52nd International Astronautical Congress
1-5 October, 2001/Tolouse, France

PRELIMINARY RESULTS OF THE SOUNDING ROCKET EXPERIMENT ON OSCILLATORY MARANGONI FLOWS IN LIQUID BRIDGE

R. SAVINO, R. MONTI, M. LAPPA
Università degli Studi di Napoli "Federico II"
Dipartimento di Scienza e Ingegneria dello Spazio "Luigi G. Napolitano"
P.le V.Tecchio 80, 80125 Napoli (Italy)

D. CASTAGNOLO, R. FORTEZZA
MARS Center
Via Emanuele Gianturco 31, 80142 Napoli (Italy)

Abstract

This paper reports on the results of the experiment PULSAR (Pulsating and Rotating Instabilities in Oscillatory Marangoni Flows), performed on the MAXUS 4 sounding rocket launched in April 2001 from the Swedish base in Kiruna. Aim of the experiment was the analysis of the three-dimensional and time-dependent flow regimes arising in a liquid bridge of Silicone oil when the temperature difference between the disks is increased. Pulsating and rotating oscillatory regimes have been established during the microgravity time at different temperature differences across the liquid bridge. The oscillatoy flow has been detected by visual observation of the flow field organization (using a CCD camera and silver-coated tracers), by the behaviour of the temperatures, measured by thin thermocouples at different azimuthal coordinates, and by the evolution of the surface temperature distribution, measured by an infrared camera.

1. Introduction

The stability of Marangoni convection in non-isothermal liquid bridges with cylindrical free surfaces has been the object of many researches in last years.
A liquid bridge between two differentially heated disks is a typical model for the study of Marangoni flows, their stability and their bifurcations.
Experiments performed on ground and in microgravity and numerical studies have shown the transition from the axisymmetric state to a 3-D oscillatory state and multi-morphological features of the three-dimensional oscillatory flows when a threshold temperature difference between the supporting disks is exceeded. A number of experimental works on the subject have been performed, on ground and in microgravity conditions, by different investigators [1-8].
From the theoretical/numerical point of view oscillatory thermocapillary flows in liquid bridges have been investigated by the linear stability theory [9-10] and non-linear numerical simulations, that predict steady bifurcations at low Prandt numbers [11-12] and different oscillatory flow regimes, pulsating or rotating at large Prandtl numbers (Pr >>1) [13-15].
In the latter case, the three dimensional supercritical state after the onset of oscillatory instability can be interpreted as a superposition of two counter-propagating waves, characterized by an axial and an azimuthal component, with a front wave forming a certain angle with the axis of the bridge.
When the two waves have equal amplitude a "standing wave" regime is established, with disturbances pulsating at fixed azimuthal positions. The superposition of waves with different amplitude gives rise to a "traveling wave", in which the disturbances rotate in the azimuthal direction.

2. Pulsating and rotating regimes

Figures 1 and 2 show schematically the temperature disturbances behaviour in the pulsating and rotating regimes, when the azimuthal wave number is m=1.

In the pulsating regime the temperature disturbance consists of a pair of spots (hot and cold) pulsating at fixed azimuthal positions along the interface. As explained in [14] this mechanism is evident in the time-dependent behaviour of the temperatures in the horizontal cross-sections (see Fig. 1) and along the liquid bridge interface. The spots are responsible for thermocapillary forces in the azimuthal direction, causing a pair of counter-rotating vortex cells in the transversal section (Fig. 1). At time $t=t_o$ (or $t=t_o+\tau$, where τ is the oscillation period) two azimuthal surface tension-driven jets originate at the hot spot and merge at the cold one. Mass conservation establishes a radial return flow close to the cold spot. Since the radial flow is associated with an axial flow in the negative direction, the descending radial flow transports hot fluid from the upper bulk flow to the surface at, generating at time $t=t_o + \tau/2$ a hot spot near the free surface. This spot, initially weak, grows at the expense of the cold spot until the cold spot vanishes at time $t=t_o + 3\tau/4$.

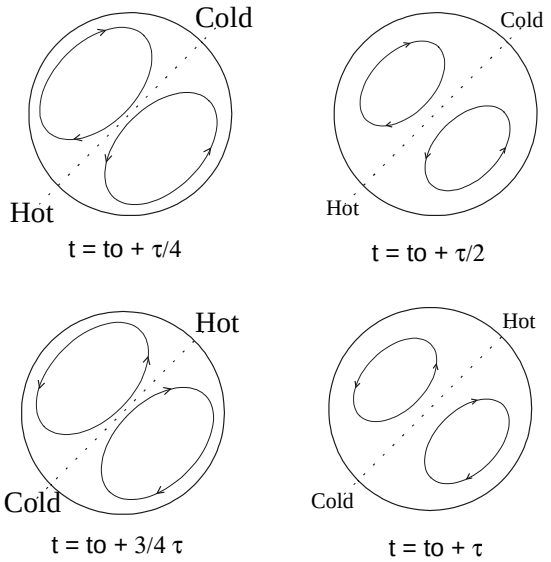

Fig. 1 Oscillatory behaviour in the pulsating regime (m=1)

A similar behaviour is observed for the cold spot.

Marangoni effects support this dynamical mechanism so that the spots pulsate (the hot spot replaces the cold one and vice versa).

In the rotating regime (Fig. 2) the temperature disturbance consists of a pair of spots (hot and cold) rotating along the circumference of the liquid bridge.

From the experimental point of view, the traveling wave model was observed by different investigators on ground and in microgravity [2-3]. The standing wave model, instead, has been observed more recently in ground-based experiments [4-6] and during Spacelab and a Maxus experiments in space [7-8]. However, open questions remain related to accuracy of the critical Marangoni numbers, how fast and what type of supercritical flow (pulsating or rotating) prevails under different conditions, especially at large Prandtl numbers.

The development of supercomputers and of efficient numerical methods allowed direct numerical solutions of the three-dimensional and time-dependent Navier Stokes equations, where the pulsating and rotating regimes appear to be two consecutive transitions of the Marangoni flow [13-15].

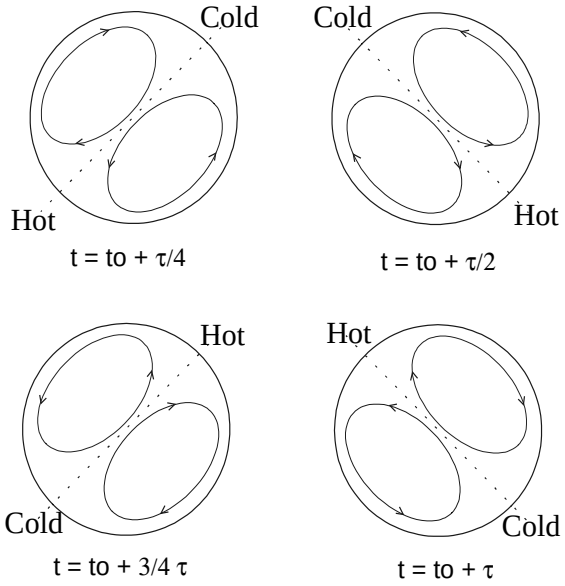

Fig. 2 Oscillatory behaviour in the rotating regime (m=1)

To investigate these behaviour, an experiment has been performed onboard the MAXUS 4 Sounding Rocket, launched in Spring 2001 from the Swedish base in Kiruna. Main objectives of the experiment were:

1) to study the transition from the axisymmetric to the oscillatory three-dimensional pulsating state
2) to investigate the transition from the pulsating to the rotating regime and to correlate experimental and numerical results
3) to analyze the main features of the 3D pulsating and rotating regimes

3. Flight hardware

The experimental apparatus is an improved version of the TEM 06-4 that has already been used during previous experiments on Texus and Maxus missions [8].
A pressurized test cell contains the liquid bridge (Silicone oil with kinematic viscosity of 2 Cs) between two disks (L=D=20mm) formed after the microgravity conditions are established. The liquid reservoir, sealed during the acceleration phase, is opened by an electromechanical device and the exact quantity of liquid needed to form a cylindrical liquid bridge is pushed between the two copper disks while the disks are moving to reach the prescribed distance. An active cooling/ heating system, based on Peltier elements, allows to control the temperatures of the two disks, imposing symmetric temperature profiles with respect to the initial temperature.
Eight thin thermocouples protrude in the bridge by 2mm in the axial direction, at the same radial coordinate (r=0.9mm), but at angles of 45 degree.
The surface temperature distribution is measured with a thermograph (FLIR SC3000), operating in the long wave infrared band (around 9microns). Two infrared mirrors on the left and on the right of the liquid bridge are used to cover a large portion of the cylindrical surface of the liquid bridge. The thermocamera is able to generate and to transmit on ground pictures at 15 fps and stores onboard digital images at 1 fps on a flash memory. The flow strucure in a meridian plane has been observed by a CCD camera using silver-coated tracers illuminated by a laser light sheet. The heat fluxes through the upper and lower disks have been measured using calibrated thin foils.

4. Results and discussion

4.1 Experimental procedure and detected oscillatory regimes

Figure 3 shows the time history of the disk temperatures during the microgravity experiment.
The experiment chamber was thermostated at 35 °C prior to lift off. The liquid bridge was formed injecting the silicone oil between the two metallic disks 100[s] after lift-off.
The zone length, of 20[mm], has been established moving the upper piston with a velocity of 0.33 [mm/s]
The temperature difference between the disks has been increased heating one disk and cooling the other one, with respect to the ambient temperature, using symmetric ramps.
An initial temperature difference $\Delta T = 5$[K] was established by means of symmetric ramp (with temperature ramps of ±0.2 [K/s]) and held constant for about seconds 200 seconds, from MET=130 to MET=330.

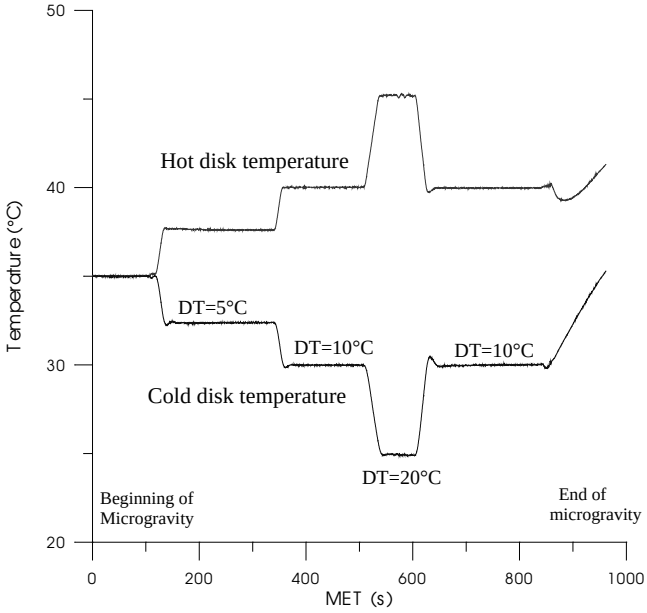

Fig 3. Disks temperature setting during the Pulsar experiment.

The temperature difference was then raised to ΔT= 10 [K] (with a ramp of ± 0.2[K/s]) and maintained from MET=350 to MET=500.
The temperature difference was raised to ΔT= 20 [K] until MET=600 and then reduced again to 10 [K] (±0.3[K/s]). This final value of ΔT was held constant until the end of the microgravity period, i.e. MET=856.
As predicted by the numerical simulations, a transition from the axi-symmetric to a pulsating three dimensional regime was detected for ΔT = 5[K]. In this regime the temperature profiles have small oscillation amplitudes (with oscillation period of about 30[s]), but the temperature oscillations, the thermocamera and the CCD images exhibit a behaviour similar to the one observed for ΔT = 10 [K], for MET=250 and MET=480.

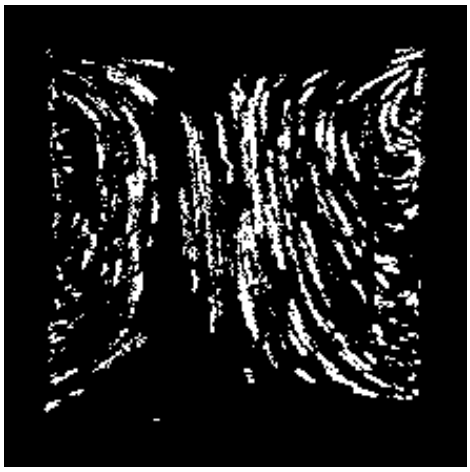

$t=t_0$

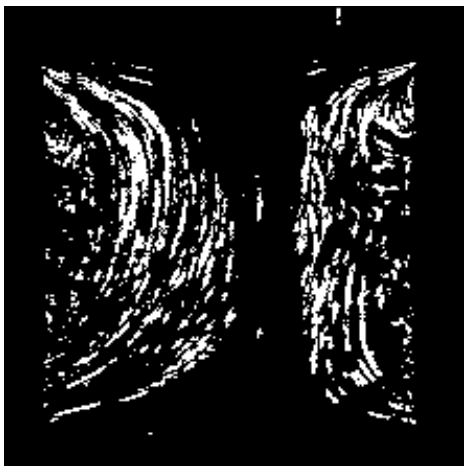

$t=t_0 +\tau/2$

Fig. 4. Tracers trajectories during half period (τ=26s) (MET=506 and 519)

The pulsating regime is characterized by the existence of a fixed pulsation plane; the axis of the deformed Marangoni toroidal convection roll, inclined with respect to the zone axis due to the onset of instability, oscillates in this plane forward and backward. Observations in direction orthogonal to this plane (see Fig. 4) show a pendular motion (with period of about 26[s]) of the branching streamlines that divide the two asymmetrical convection cells in the meridian plane.
Figure 4 shows the tracers trajectories in the meridian plane illuminated by the laser beam for ΔT=10[K]. The initial time t_0 corresponds to MET= 450.
This behaviour is basically confirmed by the thermocamera images captured at some relevant moments during the oscillation period (Figure 5). The images in Fig. 5 are obtained by black and white reproduction of the coloured thermocamera images representing the temperature disturbances on the liquid bridge surface.
To show the oscillatory behaviour of the temperature disturbances, the images shown in Figs. 5 and 6 have been obtained subtracting a suitable reference image from the contours showing the surface temperature distributions. Fig. 5 clearly shows the pulsation of the hot and cold spots in the central part of the thermocamera image and in the mirrors. Since each (cold or hot) spot shown in Figs.5 has an angular extension of 180 degree, the wave number associated to the distorted temperature field is m=1.
When the temperature difference was raised to ΔT=20[K] a transition from the pulsating to a rotating regime was identified (Fig. 6).
The rotation of the temperature disturbances along the liquid bridge interface was evident both in the frontal view and in the left and right mirrors, as shown in Fig. 6.
In this case the surface temperature distribution was found to be more complex than that observed in the case ΔT=10[K]. The resulting temperature field was given in fact by the superposition of m=2 disturbances to the basic m=1 ones . This behaviour is particularly clear in the left and right mirrors of Fig.6 where two spots (one cold and the

other hot) can be seen to be present in an angular extension corresponding to 180 degree at some relevant moments during the oscillation period, thus proving that the field comes from the sum of two differently m-based temperature distributions (m=1 and m=2).

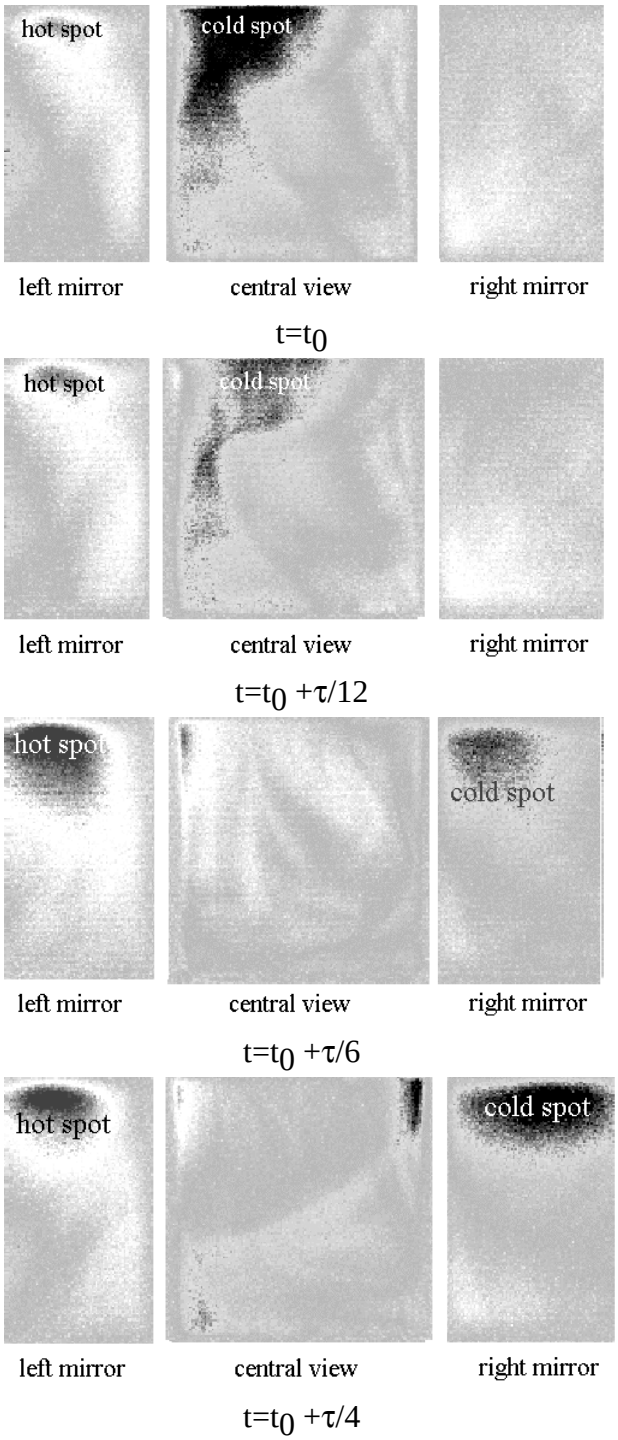

Fig. 5 Surface temperature disturbances at some relevant moments during the oscillation period (τ=22.7s) in the pulsating regime (ΔT=10[K[)

When the temperature difference was reduced again to ΔT=10[K] then a rotating flow regime (different from the pulsating regime established at the same temperature difference between MET=350 and MET=480) was observed.

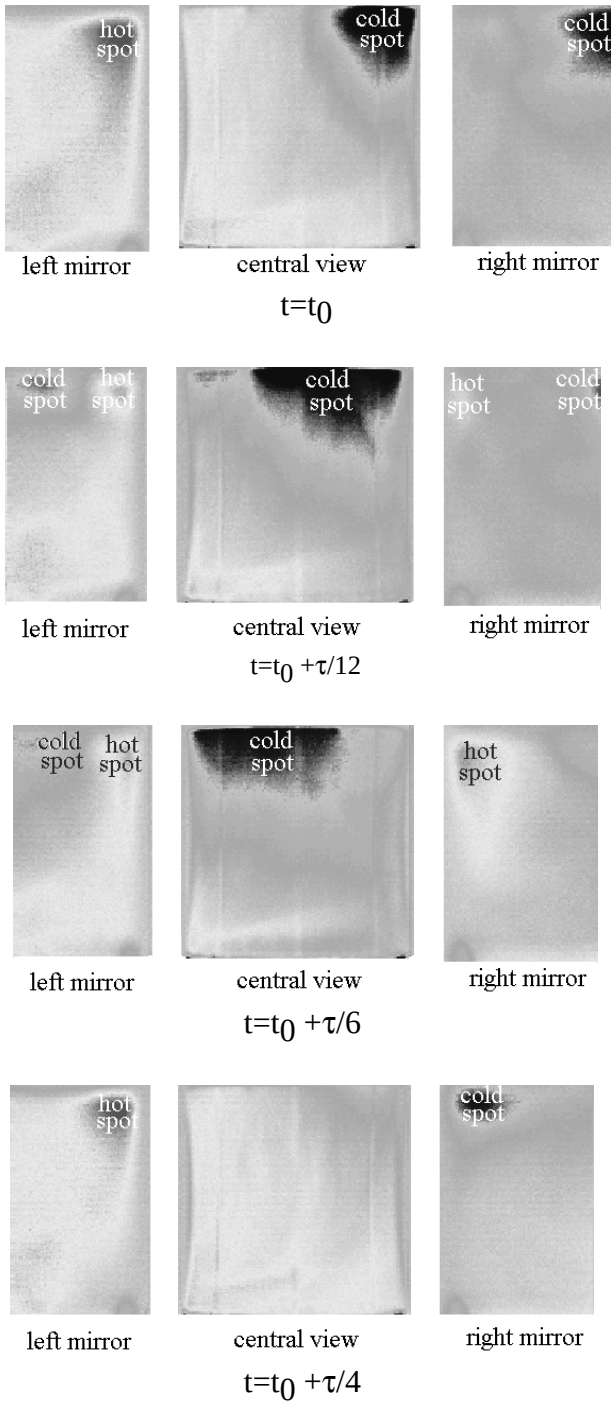

Fig. 6 Surface temperature disturbances at some relevant moments during the oscillation period (τ=23.2s) in the rotating regime (ΔT=20[K[)

The thermographic images will be further discussed in the next paragraph, in connection with the analysis of the temperature profiles.

4.2 Analysis of the temperature profiles

As discussed in the paragraph 4.1, for ΔT=5 [K] (between MET=130 and MET=330) temperature oscillations have been detected with small amplitudes (of the order of 0.2-0.4 °C). The temperature profiles exhibit a behaviour similar to the profiles measured between MET=350 and MET=480, when a temperature difference ΔT=10 [K] was established (an azimuthally standing wave with wavenumber m=1 was observed). However, for ΔT=5 [K] the main oscillation period is of about 30[s].
Fig. 7a shows the output of the thermocouples TZ1 between MET=380 and MET=480. The Fourier spectrum of the temperature profile shows that the oscillatory flow pattern is characterized by a fundamental frequency f_0=0.044 [Hz] (corresponding to a period $\tau_0 \cong 23$ [s]) and its double $f_1=2\ f_0$=0.088 [Hz].

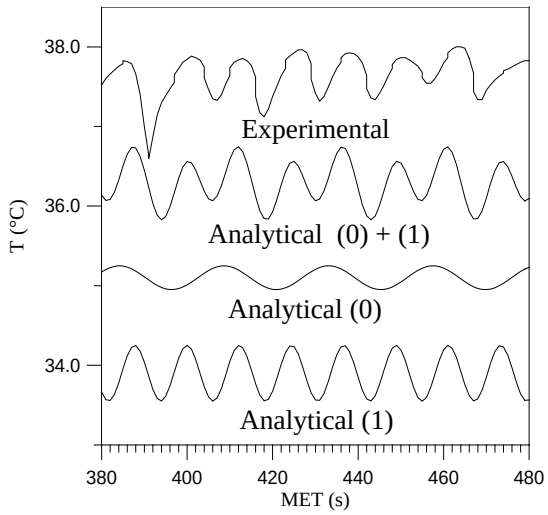

Fig 7a Temperature profile of the thermocouple TZ1, between MET=380 and MET=480 (ΔT=10K); the experimental profile is well fitted by the analytical function including only the two main fundamental harmonics.

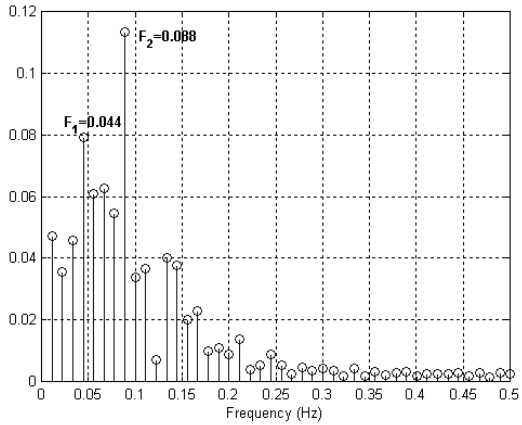

Fig 7b Fourier spectrum of the thermocouple TZ1, between MET=380 and MET=480 (ΔT=10K)

In order to understand the spatio-temporal organization of the oscillatory fields related to the above frequencies, a Fourier analysis has been performed to evaluate the different contributions related to the different harmonics. Fig. 7a shows that the measured temperature profile is well represented by the analytical function including only the two main fundamental harmonics (with frequencies f_0 and f_1).
According to the thermocamera images shown in Figs.5, the temperature disturbances exhibit a pulsating behaviour. In particular, the contribution related to the frequency f_0 has the form:

$$\tilde{T}_0(t, \theta) = A_0 \cos(m\theta)\cos(2\pi f_0 t)$$
with m=1

where θ is the azimuthal coordinate, m is the wave number, t is the time, f_0 the oscillation frequency and A_0 the oscillation amplitude related to the first harmonics.
According to the above equation, Fig. 8 shows that the contributions to the temperature profiles, related to the fundamental frequency f_0, have different amplitudes and only discrete phase shifts.
As discussed below, the thermocouples have the same axial and radial coordinates, but different azimuthal coordinates.

They are numbered consecutively counterclockwise, from TZ1 to TZ8. Four signals (TZ1, TZ2, TZ7, TZ8) have the same phase [8]; the phase shift is equal to π with the other four thermocouples (TZ3, TZ4, TZ5, TZ6).

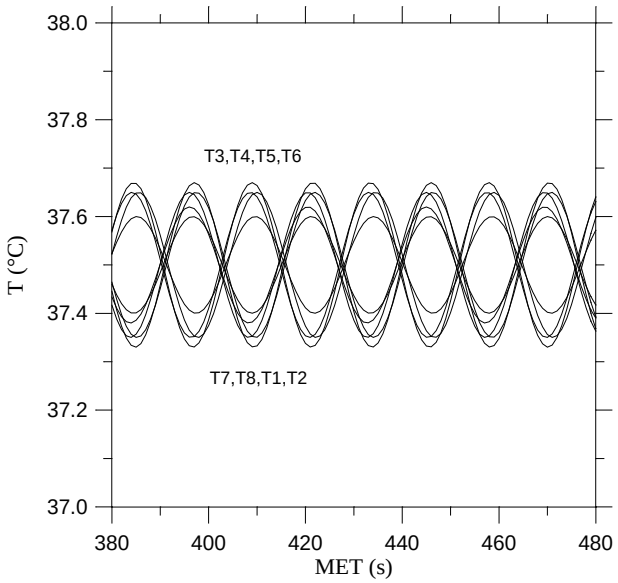

Fig. 8. Contributions from the fundamental harmonics (f_0) to the temperature profiles measured by the eight thermocouples between MET=380 sec and MET=480 (ΔT=10[K])

This behaviour is due to the fact that each temperature spot has a fixed azimuthal position and an angular extension of 180° (see Figs.5 where the standing wave regime for m=1 is shown) so that four thermocouples lie on a spot and the other four are located on the opposite spot.

Fig. 9 shows the contributions to the temperature profiles related to the harmonics with frequency $f_1=2\ f_0$.

Similarly to the contributions related to the fundamental frequency, only two values of the phase shift are allowed and four signals (TZ1, TZ2, TZ7, TZ8) have the same phase; the phase shift is equal to π with the other four thermocouples. This means that the wave number for this pulsating regime is m=1 as for the previous case.

The temperature disturbance related to the second harmonics can be described as

$$\tilde{T}_1\ (t, \theta)= A_1 \cos(m\theta) \cos (2\ \pi\ f_1\ t)$$
$$\text{with } m=1 \text{ and } f_1=2\ f_0$$

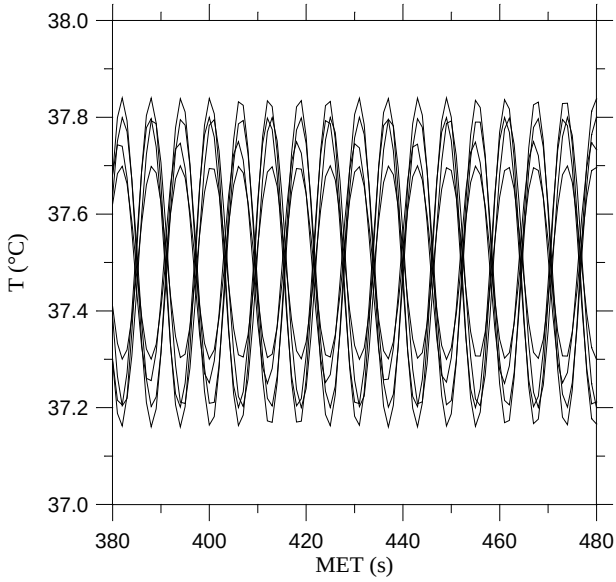

Fig. 9. Contributions from the harmonics with frequency $f_1=2\ f_0$ to the temperature profiles measured by the eight thermocouples between MET=380 sec and MET=480 (ΔT=10[K])

As a consequence, the pulsating behaviour in the azimuthal direction can be simply described as :

$$T(t, \theta)=T_{ave}+A_0 \cos(m\theta) \cos (2\pi\ f_0 t) +$$
$$A_1 \cos(m\theta) \cos(4\pi\ f_0 t)$$

Where T_{ave} is the time-average temperature in the cross section, at fixed r and z.

As discussed in paragraph 4.1, for ΔT=20[K] a transition from the pulsating to the rotating regime has been detected.

The Fourier analysis of the thermocouples signals (Fig. 10) shows that, together with the fundamental frequency (f_0=0.043 [Hz]) and with the harmonics with $f_1=2\ f_0$=0.086 [Hz], an additional harmonics is evident with frequency $f_2=2\ f_1=4\ f_0$=0.16 [Hz].

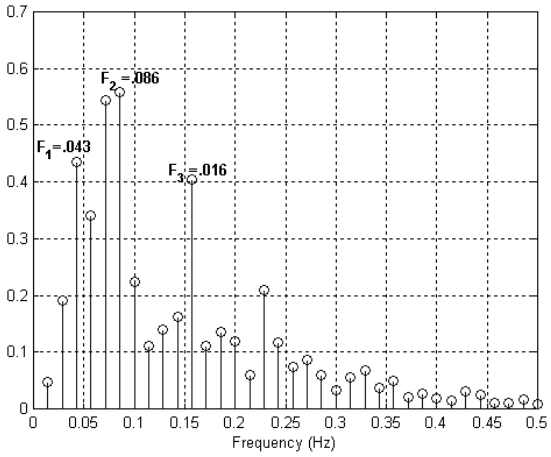

Fig 10. Fourier spectrum of the output of the thermocouple TZ1, between MET=540 and MET=620 (ΔT=20[K])

The contributions to the time temperature profiles related to the different harmonics show a phase displacement depending on the azimuthal co-ordinate, proving that the regime is rotating. This is shown in Figs. 11 and 12 for the contributions related to the frequencies f_1 and $f_2 = 2\,f_1$, respectively.

When the behaviour of the harmonics with frequency f_1 is considered, the phase shift between two thermocouples at 45°, 90° and 180° is π/4, π/2 and π, respectively (see Fig. 11), showing that the wave number associated to this harmonics is m=1.
The corresponding thermo-fluid-dynamic field is characterized by rotating temperature disturbances in the form:

$$\tilde{T}_1(t,\theta) = A_1 \cos(m\theta + 2\pi f_1 t) \quad \text{with } m=1$$

This means that two thermocouples located at the same axial and radial co-ordinates, but at different azimuthal co-ordinates, oscillate synchronously with the same frequency and a phase shift equal to the azimuthal distance.
When the behaviour of the second harmonics is considered (Fig. 12), the phase shift between two thermocouples at 45°, 90° and 180° is π/2, π and 2π, respectively, showing that the wave number associated to this harmonics is m=2. The thermo-fluid-dynamic field is characterized by rotating disturbances in the form:

$$\tilde{T}_2(t,\theta) = A_2 \cos(m\theta + 2\pi f_2 t) \quad \text{with } m=2$$

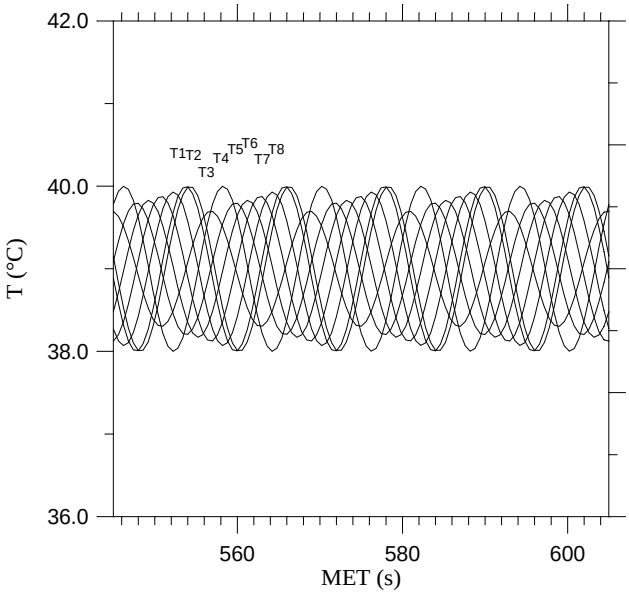

Fig 11 Contributions from the harmonics with frequency f_1 to the temperature profiles measured by the eight thermocouples between MET=545 and MET=600 (ΔT=20K, m=1)

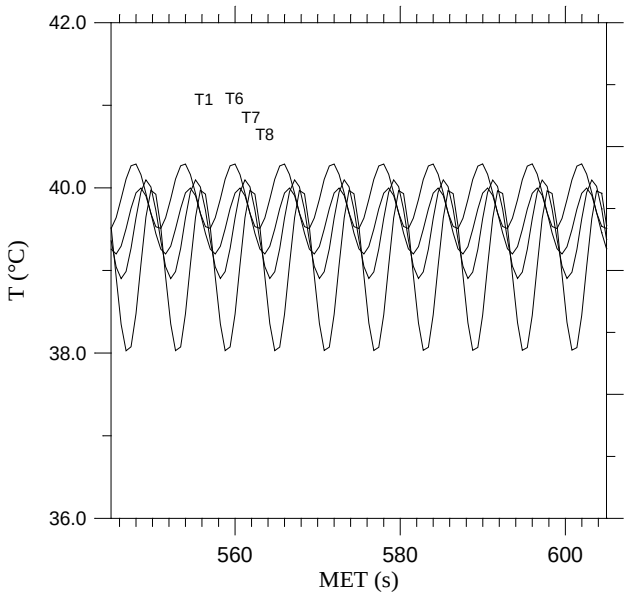

Fig 12 Contributions from the harmonics with frequency f_2 to the temperature profiles measured by the eight thermocouples between MET=545 and MET=600 (ΔT=20K, m=2)

When the temperature difference was decreased from ΔT=20[K] to ΔT=10[K] a rotating regime was still found, as shown in Figs. 13-15. The thermocouples exhibit a continuous phase shift; the fundamental frequency, however, was found to be decreased with respect to the pulsating regime previously found at ΔT=10[K]. This proves that, for a fixed imposed temperature gradient, the fundamental frequency is influenced by the spatio-temporal oscillatory regime (f_0=0.044 Hz during the pulsating regime and f_0=0.037 Hz during the rotating regime).

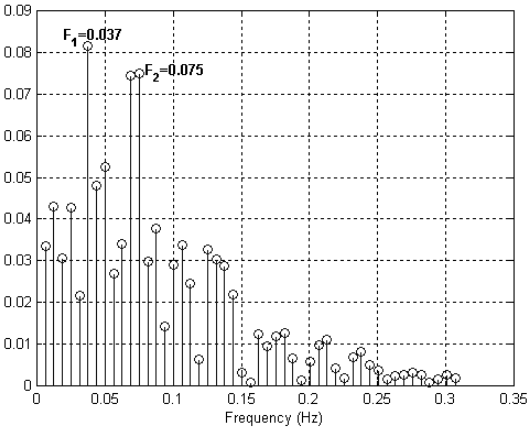

Fig 13. Fourier spectrum of the output of the thermocouple TZ1, between MET=620 and MET=856 (ΔT=10[K])

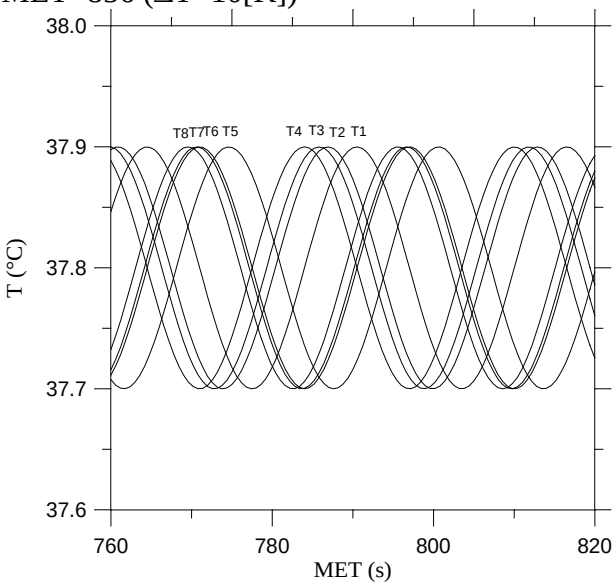

Fig 14 Contributions from the harmonics with frequency f_0 to the temperature profiles measured by the eight thermocouples between MET=760 and MET=820 (ΔT=10K, m=1)

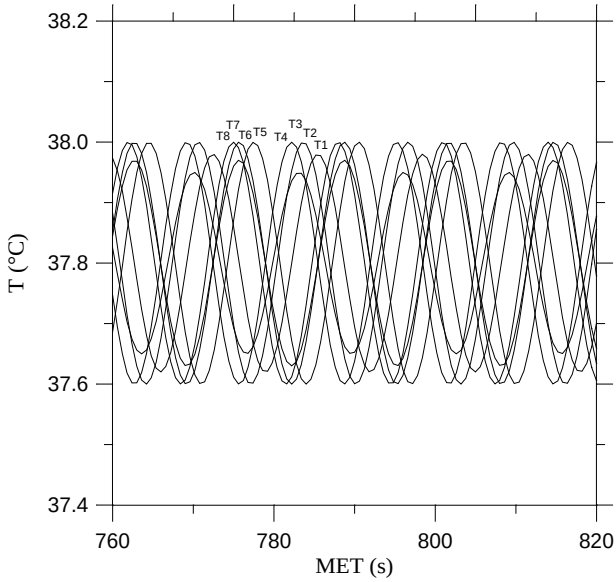

Fig 15 Contributions from the harmonics with frequency f_1 to the temperature profiles measured by the eight thermocouples between MET=760 and MET=820 (ΔT=10K, m=1)

4.3 Analysis of the heat fluxes

Figure 17 shows the measured heat fluxes on the top and bottom disks during the entire experiment. The measurement is made by the heat fluxmeters described in [8]. The heat flux on the hot disk is systematically higher than the flux on the bottom disk and the difference (of the order of 0.1W) is much larger than the estimated radiative heat flux from the cylindrical liquid surface towards the ambient. From the energy balance equation in the liquid bridge the difference between the heat fluxes across the two disks (at steady state) has been explained by the partial evaporation of the oil from the lateral interface. In fact, a careful analysis of the CCD images shows a volume reduction of the liquid bridge of about 0.8 [cm^3] in 700 [s], resulting in an average evaporation rate J_V of the order of 10^{-3} [g/s]. This corresponds to an average heat flux $Q= J_V$ x Hv = 0.13 [W] (H_V=130 [J/g] is the enthalpy of vaporization of the oil, see [16]). This value is in quantitative agreement with the measured difference between the heat fluxes across the two disks.

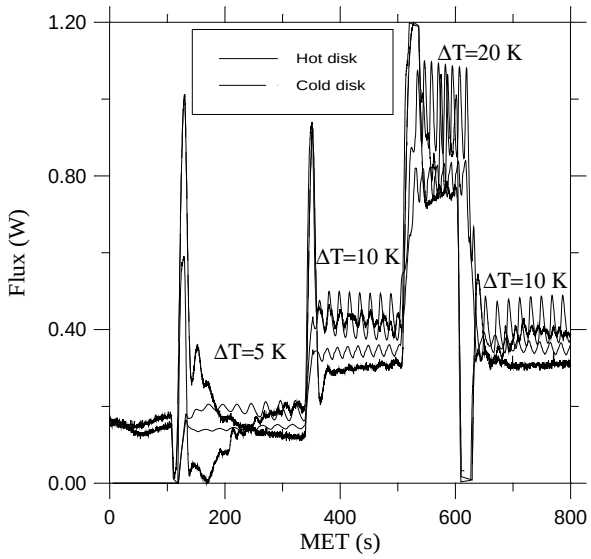

Fig. 16 overall heat fluxes across the two disks.

4.4 Numerical correlation

The method used for the present numerical simulations is described elsewhere (see e.g. [14]).
The code has been used to compute the three-dimensional thermofluidynamic field in the liquid bridge at the experimental conditions (ΔT=5[K], 10[K], 20[K]).

The numerical simulations have shown that the presence of a heat flux from the lateral interface towards the ambient (caused, as seen, by the partial oil evaporation) has a great influence on the flow field regimes established in the liquid bridge.
In particular, the pulsating regime is strongly stabilized for ΔT=5[K] and ΔT = 10[K], in comparison to the case of an adiabatic cylindrical interface.
The numerical simulations carried out for ΔT = 10[K] in the case of adiabatic surface have shown in fact a very complex frequency spectra (i.e. a chaotic behaviour) and a rotating regime from the beginning. In the case of non-adiabatic interface for ΔT=5[K] and ΔT=10[K] a stable pulsating regime has been obtained for the entire duration of the experiment (t=800 s) and the frequency spectra is very regular (only two frequencies).
At ΔT=20[K] however, though the presence of a heat flux from the lateral interface towards the ambient, the numerical simulations predicts a rotating regime from the beginning.
The numerical and experimental results are summarized in Table I.

	Conditions	Flow regime	Main period	Number of harmonics
ΔT=5 K	Numerical (q=0)	Pulsating	25 [s]	1
	Numerical (evaporation)	Pulsating	28.8 [s]	2
	Experimental	Pulsating	30 [s]	2
ΔT=10 K	Numerical (q=0)	Chaotic Rotating	24.9 [s]	> 4
	Numerical (evaporation)	Pulsating	26.7 [s]	2
	Experimental [350-500s]	Pulsating	22.7 [s]	2
	Experimental [600-800s]	Rotating	27.0 [s]	2
ΔT=20 K	Numerical (q=0)	Chaotic	-	> 4
	Numerical (evaporation)	Rotating	27.7 [s]	3
	Experimental	Rotating	23.2 [s]	3

Table I: Flow regimes; comparison of numerical results (for adiabatic free surface and free surface with a heat flux towards the ambient due to the evaporation) and experimental results

5. Conclusions

Pulsating and rotating regimes have been detected from the visual observation of the flow field (through light sheet illumination), from the analysis of the temperature profiles and from the infrared images provided by the thermograph.
The results of the microgravity experiment confirm that, as anticipated by numerical results, at the onset of the oscillatory Marangoni instability a pulsating regime, caused by a hydro-thermal standing wave, is established.
The temperature difference across the bridge was increased from 10[K] to 20[K] to accelerate the transition from the pulsating to the rotating regime. When the temperature difference was reduced again to 10[K] a rotating regime was finally established.
The frequencies and the related wavenumbers in the different supercritical flow regimes have been studied through a Fourier analysis of the temperature profiles and confirm the CCD and the thermocamera images.
Further numerical simulations are in progress to correlate the experimental results.

Acknowledgements

The authors wish to thank the Italian Space Agency (ASI) for the financial support and the ASTRIUM technical staff for the support during the preparation and execution of the experiment.

6. References

[1] D. Schwabe, A. Scharmann, F. Preisser, R. Oeder 1978, Experiments on surface tension driven flow in floating zone melting, J. Crystal Growth **43**, 305-312
[2] R. Monti 1987, On the onset of the oscillatory regimes in Marangoni flows, Acta Astronautica **15**, 557-560
[3] F. Preisser, D. Schwabe, A. Scharmann 1983, Steady and oscillatory thermo capillary convection il liquid columns with free cylindrical surface, J.Fluid Mech. **126** , 545-567
[4] R. Velten, D. Schwabe, A. Scharmann 1991, The periodic instability of thermocapillary convection in cylindrical liquid bridges, Phys.Fluids A 3, 267-279
[5] S. Frank, D. Schwabe 1998, Temporal and spatial elements of thermocapillary convection in floating zones, Experiments in Fluids, **23**, 234-251
[6] R.Monti, R.Savino, M. Lappa 1998, Scientific and technological aspects of a sounding rocket experiment on oscillatory Marangoni flow; *Space Forum*, 2, 293-318.
[7] Carotenuto L., Castagnolo D., Albanese C. and Monti R., 1998, Instability of thermocapillary convection in liquid bridges, Phys. Fluids A, **10**, 555-565.
[8] Monti R., Savino R., Lappa M., Carotenuto L., Castagnolo D., Fortezza R. , Flight results Marangoni flow instability in liquid bridge. *Acta Astronautica*, Vol. 47, N.2-9, pag. 325-224, 2000.
[9] Kuhlmann H.C., Rath H.J. 1993, On the interpretation of phase measurements of oscillatory thermocapillary convection in liquid bridges, Phys. Fluids A 5 (9), 2117-2120
[10] M.Wanshura, V. Shevtsova, H.C. Kuhlmann, H.J.Rath 1995, Convective instability mechanism in thermocapillary liquid bridges, Phys. Fluids A **5**, 912
[11] M. Lappa and R. Savino 1999, Parallel solution of the three-dimensional Marangoni flow instabilities in liquid bridges; *Int. J. Num. Meth. Fluids*, 31, 911-925
[12] M. Lappa, R. Savino and R. Monti 2001, Three-dimensional numerical simulation of Marangoni instabilities in non-cylindrical liquid bridges in microgravity; *Int. J. of Heat and Mass Transfer*, 44, Issue 10, 1983-2003.
[13] R. Savino and R. Monti, 1996, Oscillatory Marangoni convection in cylindrical liquid bridges, Phys. Fluids, **8**, N. 11, 2906
[14] M. Lappa, R. Savino and R. Monti 2001, Three-dimensional numerical simulation of Marangoni instabilities in liquid bridges: influence of geometrical aspect ratio; *Int. J. Num. Meth. Fluids*, 36 (1), 53-90.
[15] M. Lappa, R. Savino and R. Monti 2000, Influence of buoyancy forces on Marangoni flow instabilities in liquid bridges; *Int. J. Num. Meth. Heat Fluid Flow*, 10, Issue 7, 721-749
[16] N. B. Vargaftik, Y. K. Vinogradov, V. S. Yargin, 1996, Handbook of Physical Properties of Liquids and Gases: Pure substances and Mixtures, Begell House inc., New York, Wallingford